Energy performance assessment of an auto-cascade cycle for ultra-low temperatures with the pair R1150 - R600a

Rodrigo Llopis*, Manel Martínez-Ángeles, Daniel Calleja-Anta, Laura Nebot-Andrés

Thermal Engineering Group, Mechanical Engineering and Construction Department,

Jaume I University, Spain

*Corresponding author: rllopis@uji.es, +34 964 718136

Abstract

Most of the research about auto-cascade refrigeration systems for ultra-low temperature applications is performed from a theoretical perspective due to the complexity of designing, testing, and measuring systems that work in two-phase conditions in most components of the cycle. A recent developed method has provided the opportunity to understand its thermodynamic peculiarities, which generally differ from the assumptions considered in simulation. This work presents for the first time, a consistent experimental evaluation of an auto-cascade refrigeration system for space temperatures between -80 to -60 ºC. The work energetically optimizes a plant with the pair R1150/R600a using three different charging compositions (25/75%, 30/70% and 35/65%) at a heat rejection temperature of 25 ºC. Then, for the best option (340 g at 30/70%), presents the thermodynamic evaluation at three heat rejection levels (25, 30, 35 ºC) under steady-state conditions. Experimental measured COP ranged from 0.155 at a heat rejection temperature of 25 ºC to 0.087 at 35 ºC, with a rated cooling capacity decreasing from 139 W at 25 ºC to 87 W at 35 ºC.

Keywords

Auto-cascade; autocascade; COP; ultra-low temperature; R1150; R600a

Nomenclature

AC	auto-cascade refrigeration system
CHX	cascade heat exchanger
COP	coefficient of performance
E	energy consumption, kW·h
h	specific enthalpy, J·kg^{-1}
$\dot{Q}_o$	cooling capacity, W
$q_{o,vol}$	volumetric cooling capacity, kJ·m^{-3}
$\dot{m}_l$	refrigerant mass flow rate from bottom of PHS, kg·s-1
$\dot{m}_t$	refrigerant mass flow rate through compressor, kg·s-1
$\dot{m}_v$	refrigerant mass flow rate from top of PHS, kg·s-1
p	pressure, bar
P_C	power consumption, W
t	temperature, ºC; time, s
x_v	vapour title
Z	mass percentage composition of R-1150

Z_t	composition through the compressor
Z_l	composition from the bottom of PHS
Z_v	composition through the refrigerated space
$Z_{l,e}$	equilibrium liquid mass percentage composition
$Z_{v,e}$	equilibrium vapour mass percentage composition

Greek symbols

$\Delta t_{span} = t_{rs} - t_{env}$	effective achieved temperature difference
η_G	overall efficiency of the compressor

Subscripts

crit	refers to critical conditions
CHX	cascade heat exchanger
dis	compressor discharge
env	climatic chamber temperature
fan	condenser fan
HR	heat rejection temperature
in	inlet
IHX	internal heat exchanger
k	condenser
l	saturated liquid; bottom exit of PHS
o	evaporator
out	outlet
max	maximum
min	minimum
rs	refrigerated space
suc	compressor suction
v	saturated vapour; top exit of PHS
v,chx,o	state at exit of CHX at high pressure
chx,o	state at exit of CHX at low pressure
mix	mixing point before CHX

1. Introduction

Although ultra-low temperature refrigeration systems have been extensively used to cryopreserve biological material in hospitals and research centres, its interest has been renewed due to COVID-19 pandemic, as some of the most famous vaccines need to be stored and distributed in temperatures below -80ºC. According to the International Institute of Refrigeration [1], more than 7 billion COVID-19 vaccines were ordered at the end of 2020, with storage temperatures ranging from -90 to 8ºC. In addition, the pandemic highlighted the shortage of ultra-low temperature refrigeration systems worldwide, and their use is expected to grow exponentially. According to Mota-Babiloni et al. [2], and focusing on equipment with medium and low refrigeration capacity, two technologies dominate: the multi-stage cascade cycles, which employ at least two different refrigerant fluids that work in independent vapour compression cycles interconnected through recovery heat exchangers; and auto-cascade (AC) refrigeration cycles, which employ a mixture of at least two refrigerants that are fractionated internally in the refrigeration cycle. Multi-stage cascade systems are used for higher capacity appliances because they generally offer higher energy efficiency than others being able to

compensate the extra cost of more than one compressor. However, the auto-cascade refrigeration system, with reduced energy efficiency in relation to the former, is preferred for low refrigeration capacities, since it is a system that allows reaching very low temperatures using only one compressor. Recently Li et al. [3] have presented a detailed review of used refrigerant pairs, composition separation, and regulation of auto-cascade refrigeration systems.

Initial AC commercial systems for ultra-low temperature (around -80ºC) operated with the base fluids R134a as least volatile fluid (NBP = -26.36 ºC) and R23 as highest volatile one (NBP = -82.24 ºC), being the final design refined by the introduction of some other pure components. However, the F-Gas Regulation [4] started to introduce restrictions to the use of high-GWP refrigerants, like R23, and the manufactures started to move to hydrocarbon pairs: R170 and R290 is used to achieve temperatures up to -60ºC [5] and R1150 and R600a to reach temperatures near -90 ºC [6, 7]. Although the AC cycle is complex, since there is internal fractionation of the components and most of the cycle operates in two-phase condition, there are some theoretical studies aiming to foresee their operating conditions and minimum achievable temperature. Wang et al. [8] focused on the use of mixtures of ethane (R170 and R290, R170 and R600 R170 and R600a) for application up to -60ºC in a two-stage AC system with two separators, while He et al. [9] for the same pairs considered a simple AC system. Yan et al. [10] [11] considered mixtures with propane (R290 and R600, R290 and R600a) for a dual temperature refrigeration system based on a single-AC system for applications at -30ºC. Rodríguez-Jara et al. [6], Liu et al. [5] [12], Li et al. [13], He et al. [9] and Tan et al. [14] used different AC layouts and considered the mixture R1150 and R600a for temperatures up to -80 ºC.

However, from an experimental approach, the available scientific literature related with AC systems is scarce and the information about the thermodynamic operation of the cycle is usually not covered by the works, but they generally focus on the reached temperatures and on the pull-down performance. Aprea & Maiorino [15] were able to build a system for temperatures up to -150 ºC using with a non-revealed mixture of 7 components (R507, R245fa, R116, R23, R14, R744, R290) using an interesting two-stage AC system. They focused their analysis on the pull-down characteristics, the control during the start-up to avoid very high discharge pressures, and mainly on the achieved temperature. Due to the complexity of the cycle and the refrigerant mixture, they were not able to provide a COP value. Du et al. [16] developed a single-stage AC plant working with R23 and R134a, reaching -66.4 ºC. They attempted to calculate a COP using simulation but obtained large differences between the experimental results. Zhang et al. [17] built a CO_2 and R290 AC and tried to validate an experimental COP with simulation, but, as with previous authors, there was a large deviation. Recently, Bai et al. [18] [19] using a single-stage ejector enhanced AC with R23 and R134a evaluated the cooling capacity and the COP of the cycle by calculation of the heat transfer to the refrigerated space and the energy input from an electrical heater. Also, they mentioned that, according to the experimental behaviour, the circulating compositions would differ from the charging one, but did not provide further explanations. Finally, Llopis et al. [7] were able to develop a measurement method for a simple AC system, presented its validation and uncertainty and reported preliminary COP values for the pair R1150 and R600a [30/70 $\%_{mass}$] from 0.139 (t_{rs} = -83.0 ºC) to 0.277 (t_{rs} = -59.4 ºC) at a heat rejection level of 25ºC. Also, they confirmed the hypothesis of Bai et al. [18], demonstrating that the circulating compositions in an AC system largely differ from the charging ones.

This work focuses on the operation of an AC system with the pair R1150 and R600a and aims to enlarge the scientific knowledge of this architecture and provide experimental data for supporting simulating studies and to guide the development of AC systems. First, the manuscript discusses how the refrigerant mixture and the percentage of components influences the behaviour of the auto-cascade system; second, it describes the experimental test rig that

allows calculating the energy parameters with high accuracy and the experimental tests designed for its characterization; finally, it details the experimental evaluation and details how this system behaves and differs from the generalized theoretical assumptions. This study provides the energy optimization procedure of an AC system covering different mass charging compositions at different charges from temperatures to -80 to -60ºC at a constant heat rejection temperature of 25ºC. The work presents the first exhaustive thermodynamic evaluation up to the date of this technology.

2. Materials and methods

2.1. Experimental test rig

The auto-cascade refrigeration system used in this work is sketched in Fig. 1. Design details to perform its evaluation using the fluid pair R1150 (most volatile component) and R600a (least volatile component) are the following: Due to the absence of compressors for these types of mixtures, an R404A semihermetic compressor was selected for this application (displacement 34.38 cm^3, nominal power 1.12 kW, lubricant POE ISO22, peak pressure 28.7 bar). Its operating range in terms of pressure for R404A is in the same order of magnitude than the required for the AC application (see section 2.2). However, as described in the results section, the circulating refrigerant mass flow rate is lower when compared to that using R404A, which causes a decrease in the overall efficiency of the compressor. At the compressor exit a coalescent oil separator was used. Plant incorporates a mini-channel air condenser to perform partial condensation of the refrigerant mixture. At the exit of the condenser, the mixture is fractionated in the phase separator (PHS), where the fluid is divided into two steams: saturated vapour (*v*) flows to the cascade heat exchanger (CHX) and saturated or unsaturated liquid (*l*) goes to the internal heat exchanger (IHX). The saturated vapour (*v*), which is enriched with the most volatile component (R1150) is condensed and subcooled in the CHX and then expanded using the capillary C_2 (3.5 m long, 0.7 mm diameter) up to the low pressure. In this point (*o,i*) the refrigerant reaches its lowest temperature. Then, the mixture partially evaporates in the evaporator of the refrigerated space, which corresponds to 10 m 3/8-inch tube welded on the plate of the container. The refrigerated space has dimensions of 0.5 x 0.5 x 0.5 m and is insulated with 120 mm of high density expanded polyurethane. The current enriched with the least volatile component (R600a) is subcooled in the IHX to get some subcooling degree to guarantee accurate measurements of mass flow ($\dot{m}_l$) and density (ρ_l) in the Coriolis mass flow meter. After that, it is expanded using the capillary C_1 (3.5 m long, 0.7 mm diameter) up to the low pressure. At the exit of the capillary C_1, the steam is mixed with that coming from the refrigerated space (point *mix*) and then is evaporated in the CHX and reheated in the IHX to avoid low suction temperatures. Except for the compressor discharge, lubricant separator, condenser and PHS, all the cycle is insulated with 40 mm Armaflex isolation.

The system operates with two pressure levels but with three refrigerant steams with different compositions. The main composition which passes through the compressor and condenser is denoted as Z_t (black line Fig. 1), the one enriched with the most volatile component as Z_v (blue line Fig. 1) and that enriched with the least volatile component with Z_l (purple line Fig. 1).

The plant is instrumented, with the sensors listed in Table 1 and the positions detailed in Fig. 1. It incorporates 23 T-type thermocouples, 5 pressure gauges, a Coriolis mass flow meter and two digital wattmeters. All the information is

gathered by a cRIO-9074 daq system and handled using LabView. The plant is placed inside a climatic chamber with controlled indoor (temperature and humidity) conditions.

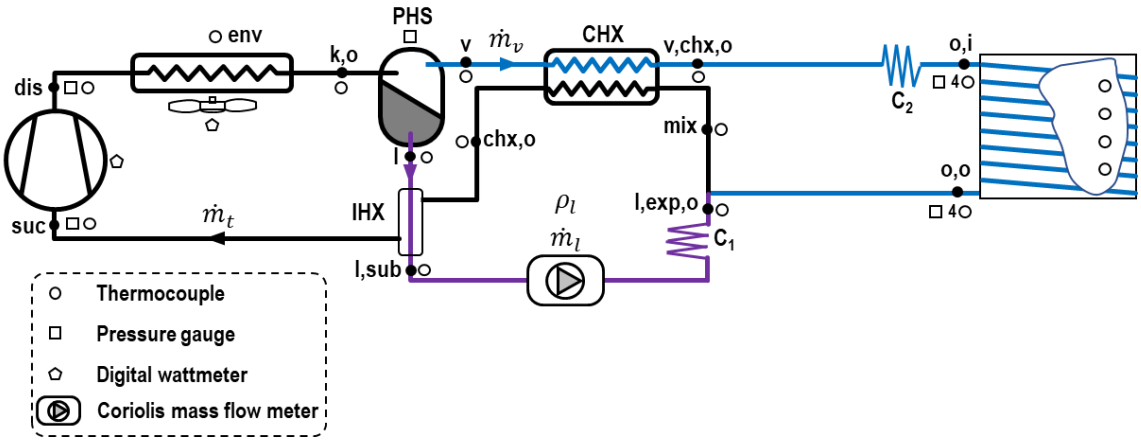

Fig. 1. Experimental test rig scheme, sensors allocation and reference points.

2.2. Refrigerant selection

By its nature, the autocascade must operate at least with a mixture of two components with distant normal boiling points, which must allow operation far away from their individuals' triple points at the desired refrigerating temperature and allow fractionation at the heat rejection temperature, as discussed by Rodríguez-Jara et al. [20]. The most used fluid pairs found in literature correspond to R23 and R134a, which is being replaced by the natural working fluids R170 and R290 for applications up to -60ºC, and R1150 and R600a for reaching temperatures up to -90 ºC.

Once the pair is selected, the determination of the proportion of the components is the most difficult and challenging aspect. This difficulty arises on the fact that in most parts of the cycle the refrigerant is in a two-phase condition and the operating pressures do not directly depend on the temperatures but on the mass charge of the system and the length of the capillary devices, thus, they correspond to two design parameters of the plant.

In relation to the heat rejection pressure, Fig. 2 illustrates the minimum and maximum concentrations of R1150 that can be used. Minimum proportion of R1150 ($Z_{R1150,min}$) is defined by the maximum heat rejection temperature ($t_{HR,max}$) and the minimum design pressure in the condenser, and maximum proportion of R1150 ($Z_{R1150,max}$) is stablished by the minimum heat rejection temperature ($t_{HR,min}$) and the maximum design pressure. The AC will fractionate (thus work) between those mass proportions but stop out of these range because fractionation will not occur. For any charging composition (or circulating, as discussed in Section 4) between those limits, the individual compositions of saturated liquid ($Z_{R1150,liq}$) and vapour ($Z_{R1150,vap}$) fractionated in the vessel will remain constant. However, charging composition will define the quantity of vapour and liquid fractionated in the phase-separator (equivalent to the relation between $\dot{m}_v$ and $\dot{m}_l$). Furthermore, for a given charging composition, an increase in the heat rejection pressure will increase the proportion of R1150 in the vapour steam. For the illustrated case in Fig. 2, for an AC working in a heat rejection temperature range between 20 to 40 ºC with a maximum steady-state design pressure of 20 bar, the mass proportion of R1150 in the mixture through the compressor and condenser must be between 10% and 75% approximately.

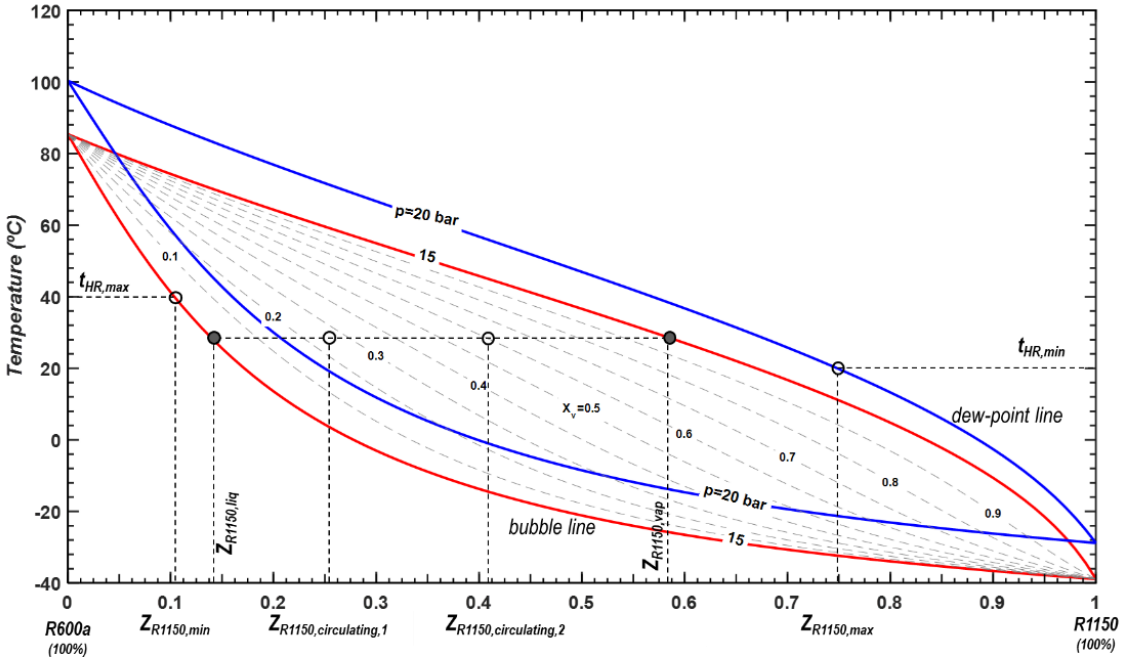

Fig. 2. Equilibrium phase diagram of binary mixtures of R600a and R1150 for constant pressure (heat rejection level)

In relation to the low operating or evaporating pressure, the circulating steam that will provide the cooling effect will have a fixed composition ($Z_{R1150,vap}$) defined by the fractionation in the phase-separator. Selection of the pressure in the evaporator (or suction) will have additional implications. As Rodríguez-Jara et al. [20] mention, the pressure in the evaporator is recommended to be higher than the atmospherics', to avoid problems with the lubricant, to have higher volumetric refrigerating effect and to avoid large compression ratios that affect the performance of the compressor. This pressure, jointly with the temperature of the refrigerant at the exit of the CHX (point *v,ch,o* in Fig. 1) will define the minimum achievable temperature and the specific cooling effect in the evaporator. Fig. 3 represents the minimum and maximum suction pressures in the AC system. The minimum achievable temperature ($t_{o,in,min}$) will be determined by the temperature at the exit of the CHX (point *v,ch,o* in Fig. 1) and the lowest working pressure. In this situation, the specific cooling effect will be the enthalpy difference until the refrigerant at the exit of the evaporator reaches the desired temperature in the refrigerated space ($q_{o.max}$). As the low pressure increases, the temperature at the inlet of the evaporator will increase and the specific cooling effect will be reduced. The limit will be the pressure at which the inlet temperature to the evaporator coincides the desired temperature in the refrigerated space ($t_{o,in,max}$). For the illustrated case in Fig. 3, for an AC capable to maintain the refrigerated space at -80 ºC with a vapour steam at the exit of the CHX at -40 ºC and 20 bar (point *v,chx,o*), the minimum selected pressure was 1 bar and the maximum 1.5 bar. For this pressure levels, for a vapor steam with 59% of R1150 and 41% of R600a, this resulted in a minimum achievable temperature at the inlet of the evaporator of -94.85 ºC with a maximum specific cooling effect of 143.0 kJ·kg^{-1} at 1 bar; and a minimum temperature of -87.4 ºC and a specific cooling effect of 99.8 kJ·kg^{-1} at 1.5 bar [21].

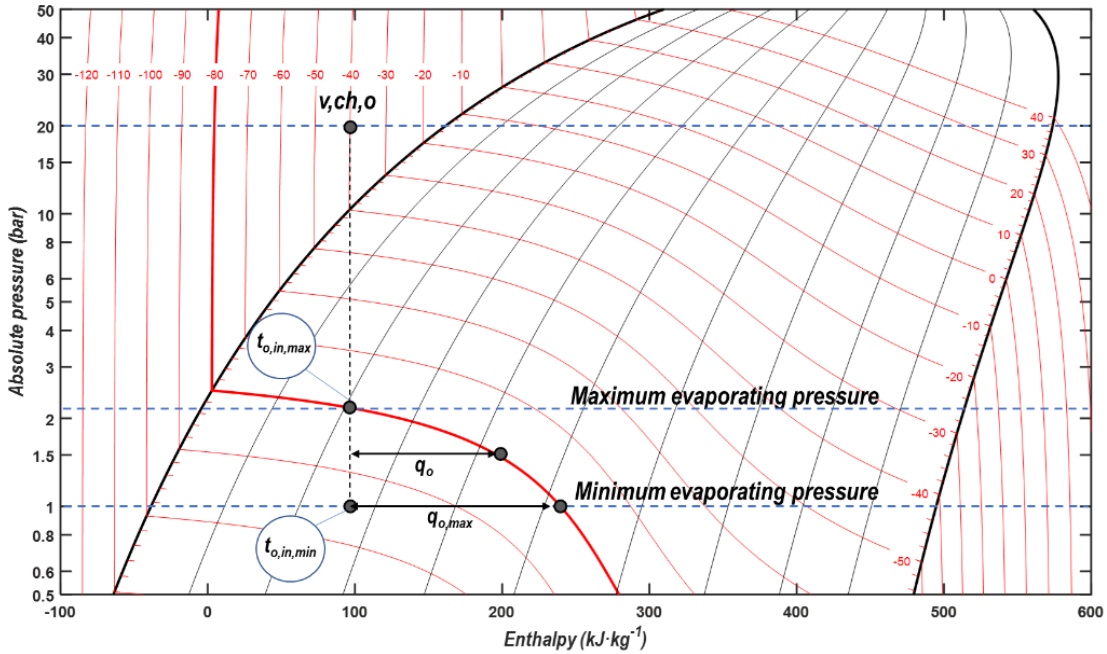

Fig. 3. Pressure-enthalpy diagram of R1150/R600a [59/41%$_{mass}$]

According to the operating conditions above mentioned, this work selected the mixtures of R600a and R1150 with the mass proportions indicated in Table 2. Properties of the main fluid (charging composition) indicate that the increase of R1150 proportion will lead to an increase of the operating pressure and an increment in the specific suction volume of the refrigerant at compressor suction. Table 2 also reflects some indicative properties when the mixture fractionates at t_{env} = 25 ºC at 15 or 20 bar. It is observed that vapour composition is identical for the three mixtures (see Fig. 2) at the same fractionation pressure, but the proportion of R1150 in the vapour steam will increase at higher fractionating pressure. The increase of fractionation pressure will allow reaching lower temperatures at the evaporator inlet and higher specific cooling capacities. However, the ratio of vapour mass steam (producing cooling effect) and the liquid mass steam will decrease with rising pressure. Combination of these effects is reflected using a definition of the volumetric cooling capacity of the AC cycle, as expressed by Eq. (*1*), where the vapour mass steam ($\dot{m}_v$) is related with the mass steam circulating through the compressor ($\dot{m}_t$) with the vapour fraction at the exit of the condenser.

$$q_{o,vol,max} = \frac{\dot{Q}_o}{\dot{m}_t} = \frac{\dot{m}_v \cdot q_{o,max}}{\dot{m}_v / x_{v_{k,o}}} = x_{v_{k,o}} \cdot q_{o,max} \qquad \text{Eq. (1)}$$

In relation to the volumetric cooling capacity, Table 2 indicates that the AC system will provide higher cooling capacity at higher pressures and higher percentage of R1150.

2.3. Experimental procedure

As mentioned, the operation of the AC system depends on three independent parameters: charging composition, fractionation and evaporator pressures. For each composition, the system was charged with different amounts of charge (from 280 g to 340 g) and then evaluated inside a climatic chamber with controlled indoor conditions.

After a vacuum procedure of at least 4 hours, charge of the system was made by introducing first the amount of R600a and then that of R1150 using a certified mass balance with 1 g uncertainty; then, the system was evaluated considering

a cycling test. The cycling test consisted of the system operation with ON / OFF compressor control with a hysteresis of -2 to 0 K in relation to the set point (t_{rs}) inside the refrigerated space. The climatic chamber was maintained always at 25 ± 0.5 ºC and the temperature of the refrigerated space was varied from -80 to -60 ºC in 5 steps of 8 hours each one. Fig. 4 details an example of the cycling tests for 320 g of the mixture R1150 and R600a [35/65 $\%_{mass}$]. Cycling test was the reference to evaluate the energy consumption and duty cycle during normal operation of the system, as well as, to evaluate other important parameters, which are discussed in Subsection 3.

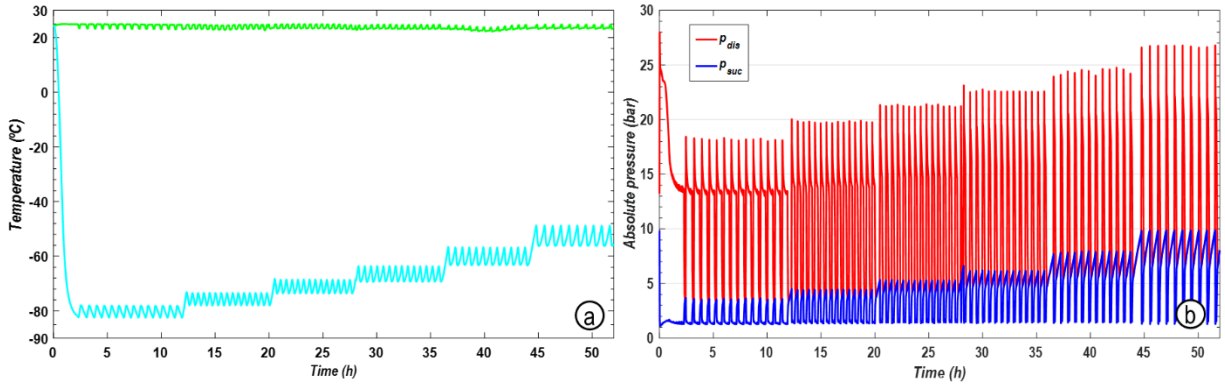

Fig. 4. Cycling test at t_{env}=25ºC with 320g of R1150 and R600a [35 / 65 %]. (a) climatic chamber and refrigerated space temperatures, (b) compressor's discharge and suction pressures

From the data obtained in the cycling test, the best configuration (charge and composition) in terms of energy consumption was selected. Later, it was subjected to a steady-state test of at least one hour to quantify the thermodynamic operating parameters. In the steady-state test, an electrical resistor controlled with an own PWM module was placed inside the refrigerated space. With the electrical load, the plant was evaluated in steady-state from the lowest achieved temperature up to -60ºC, at six temperatures. A detail of the steady-state test is shown in Fig. 5. This procedure was repeated for three temperatures of the climatic chamber (25, 30 and 35 ºC). The analysis of the best configuration is detailed in Section 4.

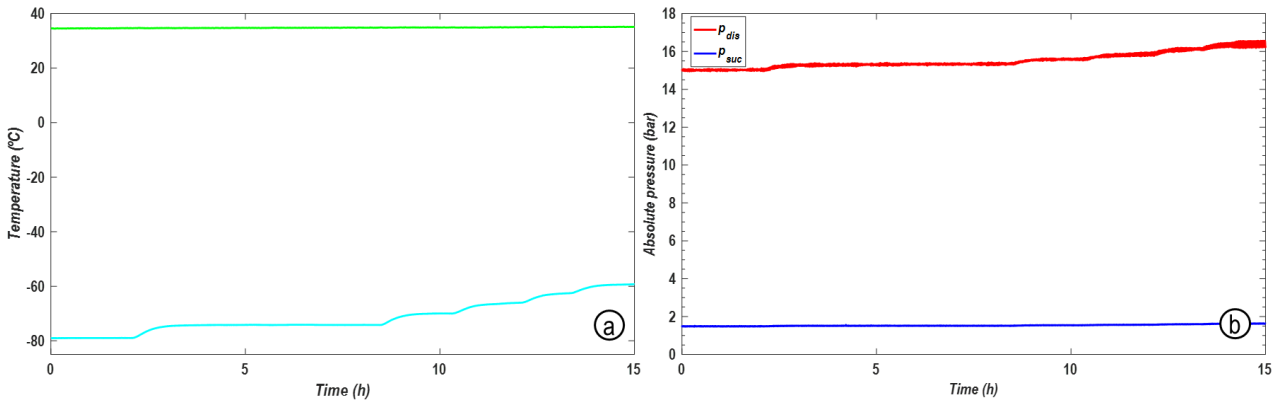

Fig. 5. Cycling test at t_{env}=35ºC with 340g of R1150 and R600a [35 / 65 %]. (a) climatic chamber and refrigerated space temperatures, (b) compressor's discharge and suction pressures

3. Energy consumption optimization

Cycling test was used to calculate the energy consumption of the AC system at different average temperatures of the refrigerated space and a constant temperature of the climatic chamber of 25 ± 0.5 ºC. Eq. (2) details the expression to compute the energy consumption from the power consumption of the compressor (P_C) using a trapezoid integration method. The measurement section considered 6 hours of cycling operation and the samples were taken every 5 seconds. Energy consumption does not account of the energy consumption of the condenser fan (it represents between 3.6 to 4.7% additional energy consumption).

$$E_i = \frac{4}{3.6 \cdot 10^6} \cdot \int_0^{6h} P_C(t) \cdot dt = \frac{4}{3.6 \cdot 10^6} \cdot \sum_{j=1}^{6h} \left\{ \left[\frac{P_C(j) + P_C(j-1)}{2} \right] \cdot [t(j) - t(j-1)] \right\} \qquad \text{Eq. (2)}$$

Fig. 6 details the energy consumption of each configuration for 24 hours and Fig. 7 the duty cycle of the compressor at different average temperatures of the refrigerated space, this last being the average temperature of the refrigerated space. Table 3 collects some operating parameters during the cycling operation.

In relation to the energy consumption and duty cycle, all combinations were able to maintain the refrigerated space at lower temperatures than -80 ºC except for 300 g 35/65 %. In addition, proportion 25/75 % presented a duty cycle higher than 80 %. Those combinations are considered no useful for the AC system. Among the rest, as seen in Fig. 6, at a set point of -80 ºC, the combinations which offered lower energy consumption were 300 g and 340 g at 30/70 %, with small deviation between them; and 280 g at 35/65 %. These combinations operated with a duty cycle around 70 %, which is considered adequate for the application. For composition 35/65 % the duty cycle increased due to higher mean temperature in the evaporator. In addition, as collected in Table 3, all combinations offered maximum discharge pressure during the start-up of the compressor inside the operating limits of the compressor. It was observed that both, when the proportion of R1150 and refrigerant charge increased, the suction pressure increased leading to high mean evaporating temperatures, worsening the heat transfer in the evaporator due to low temperature difference.

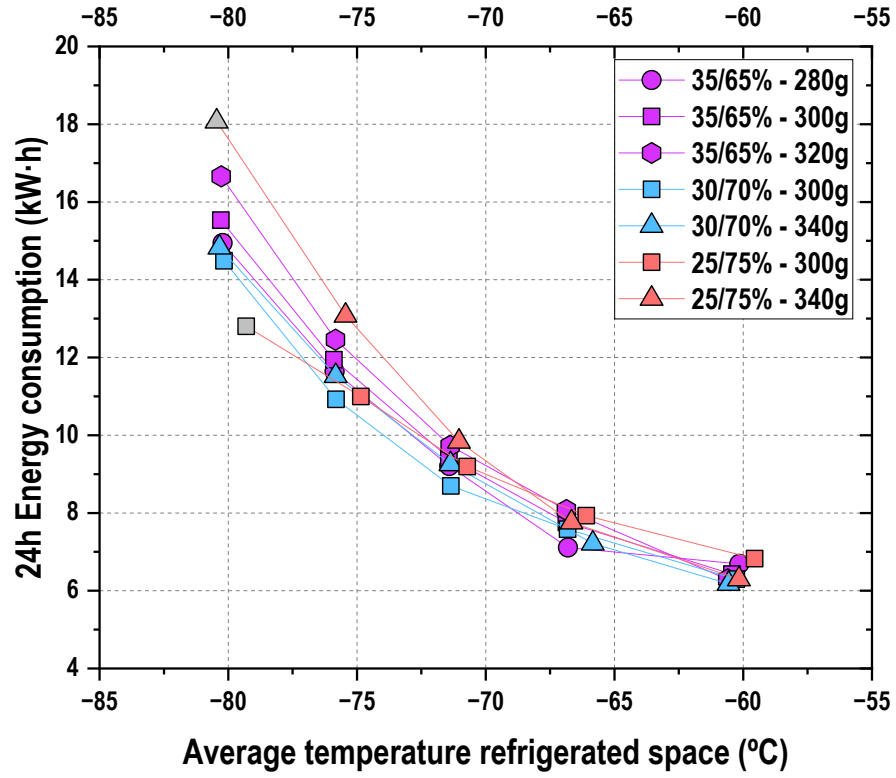

Fig. 6. Energy consumption of the AC cycle during 24 hours of operation in cycling test at t_{env}=25ºC

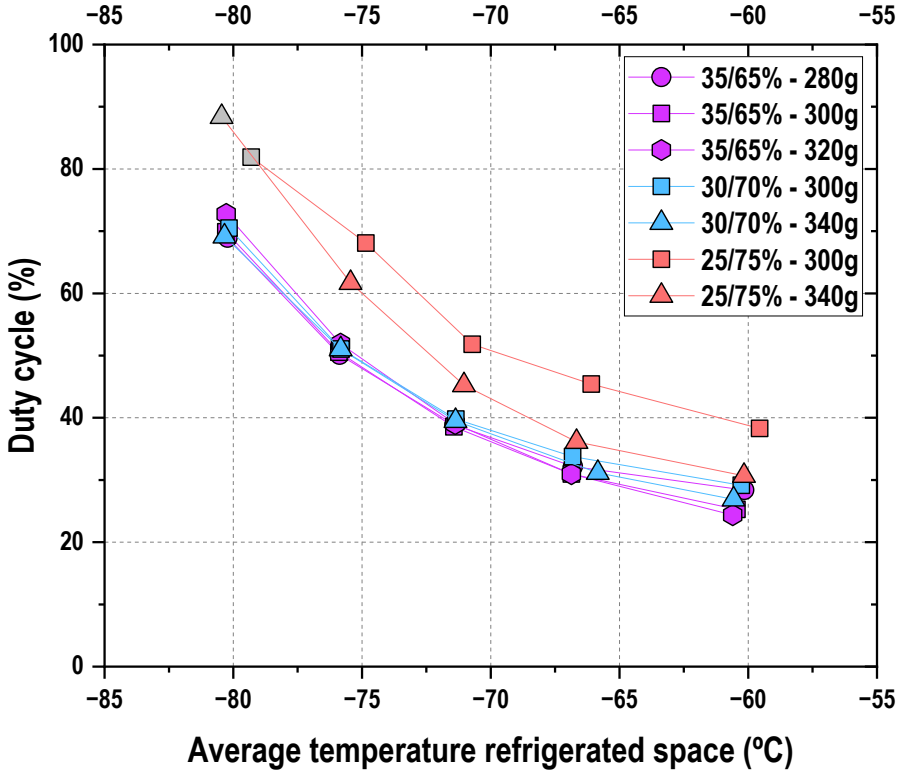

Fig. 7. Compressor's duty cycle during 24 hours of operation in cycling test at t_{env}=25ºC

4. Thermodynamic evaluation of the best configuration

The best performing combination, in terms of energy consumption was 300 g at 30/70 % at t_{rs}=-80 ºC. This combination did not provide precise measurements since did not fill completely the Coriolis mass flow meter. However, the combination 340 g 30/70 % (with 2.4 % higher energy consumption at -80ºC) provided accurate measurements of liquid density and mass flow rate. Therefore, to characterize the thermodynamic performance of the AC system, the combination 340 g at 30/70 % is selected in this section.

Evaluation of the refrigerant compositions, thermodynamic states, energy parameters and uncertainties is done with the validated method described by Llopis et al. [7], which allows their precise evaluation. Annex 1 details the uncertainty calculation of the main parameters. The combination was subjected to steady-state tests, as described in Subsection 2.3, covering temperatures of the refrigerated space from -80 to -60 ºC and climatic chamber temperatures from 25 to 35 ºC. The objective is to analyse the energy parameters and determine the dependence of the main parameters when the system operates out of the design conditions.

4.1. Refrigerant compositions

Fig. 8 presents the evaluation of the refrigerant compositions in the different flow steams calculated using the method described by Llopis et al. [7]. The first observation to be made is that the main steam (through the compressor) presents higher proportion of R1150 in relation to the charging one. For this configuration, the charging proportion was 30%. However, the circulating compositions are higher than 40% for all the range. This phenomenon was also observed by Bai et al. [18, 19] with an AC operating with R134a/R23 and by Sreenivas et al. [22] in a Joule-Thomson cycle and by Chen et al. [23] with a dual temperature refrigeration system. These authors indicated that the reason of deviation between charging and circulating compositions was the retention of one of the components of the mixture in the heat exchangers of the system. Assuming the hypothesis that, for the operation at -80 ºC (see Table 4), the mixture at the exit of the CHX (point *v,chx,o*) and at the exit of the evaporator (point *o,o*) the vapour steam is below -40 ºC and -80 ºC, respectively. At these temperatures, at a pressure of 1.4 bar, pure R600a would remain as subcooled liquid in the heat exchangers (subcooling degree of 37 K or 73 K, respectively). At this condition, R600a will be retained and only R1150 will be evaporated. This could justify the increment of R1150 in the circulating mixtures. What is important, to characterize the performance of this system, the circulating compositions must be known, since they are far away from the charging ones.

In relation to the fractionated compositions, the behaviour agrees with the reasoning of Subsection 2. On the one side, percentage of R1150 in the vapour steam (the one producing cooling effect) decreases as t_{env} rises, thus the AC system will lose the ability of producing very low temperatures (see Table 4 for the operation at -79 ºC). This percentage also rises as higher the t_{rs} is, nonetheless in this situation the achieved temperatures in the evaporator are low enough to maintain the refrigerated space. On the other side, the percentage of R1150 in the liquid steam is opposite to that of vapour's. The amount of R1150 increases as t_{env} rises, and it is maintained for all t_{rs}. It needs to be mentioned that the composition of vapour steam (Z_v) is always in agreement with that ($Z_{v,e}$) evaluated with Refprop v.10 [21]. However, the liquid one (Z_l) only agrees with that of Refprop v.10 ($Z_{l,e}$) when the liquid at the exit of the phase separator is in saturation. When saturated liquid cannot be extracted (when $x_{v,k,out}$ is high), the liquid steam presents some vapour

quality, as reflected in Table 5 for t_{env} higher than 25ºC, in this case the composition can be evaluated from the equilibrium ones given by Refprop but using Eq. (3).

$$Z_l = Z_{l,e} - x_v \cdot \left(Z_{v,e} - Z_{l,e}\right) \qquad \text{Eq. (3)}$$

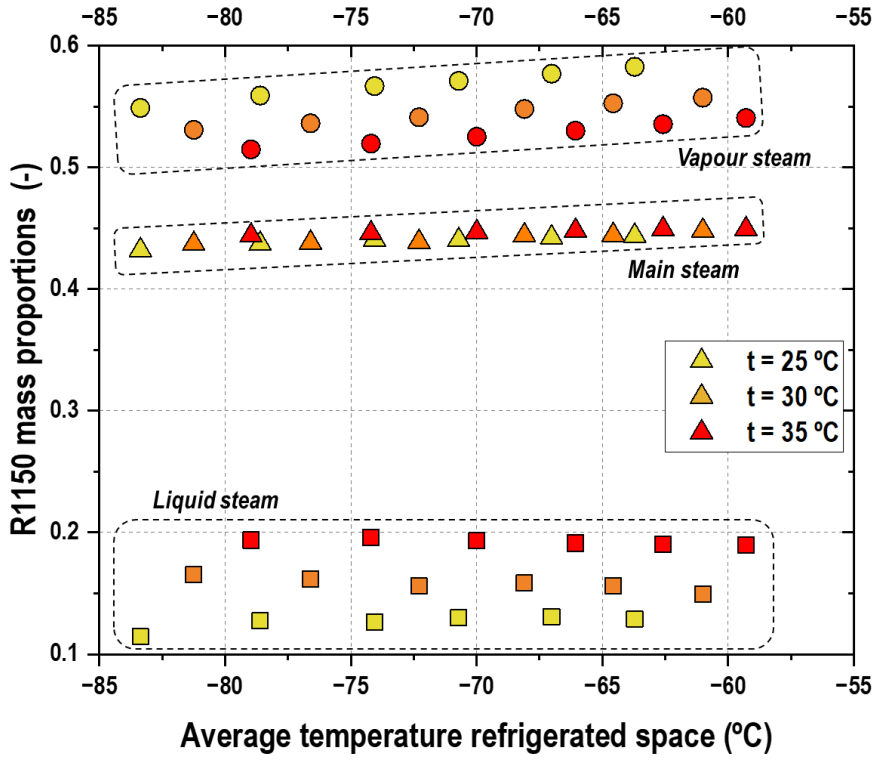

Fig. 8. R1150 mass proportion in the main steams of the AC cycle at different t_{rs} and t_{env}

To contrast the operation of the AC system with charging composition of 30/70 %, the steady-state tests near -79 ºC at the three t_{env} are depicted in Fig. 9. Compositions of each steam, pressures, temperatures, and mass flow rates are collected in Table 4 and Table 5. In relation to the compositions, the heat rejection temperature produces only significative changes in the liquid steam. At 25 ºC, the phase separator performs complete fractionation ($x_{v,l} \approx 0$), but as t_{env} increases, the vapour quality in the liquid steam rises and the percentage of R1150 in the liquid increases. The effect is a change in the saturation liquid line in the liquid steam (Fig. 9, left). However, changes in the other saturation lines are minimum. In relation to the exit of the condenser, it is appreciable that the vapor quality ($x_{v,k,o}$) rises with t_{env} indicating that $\dot{m}_v$ increases. This increase of $\dot{m}_v$ in relation to $\dot{m}_l$ implies a reduction of the subcooling degree in the CHX (point *v,chx,o*), which also reduces the capacity to provide low temperatures. Finally, it is significative the reduction of the specific cooling capacity in the refrigerated space (Fig. 9, right). Specific cooling capacity at t_{env}=25 ºC is 135.3 kJ·kg^{-1} but at 35 ºC is only 65.85 kJ·kg^{-1} (51% reduction).

To sum up, an increase of t_{env}, reduces the amount of R1150 in the vapour steam, increases the ratio $\dot{m}_v/\dot{m}_l$ limiting the subcooling in the CHX, and reduces the specific cooling effect in the evaporator. The result is a high reduction of the cooling capacity and the energy performance as t_{env} rises.

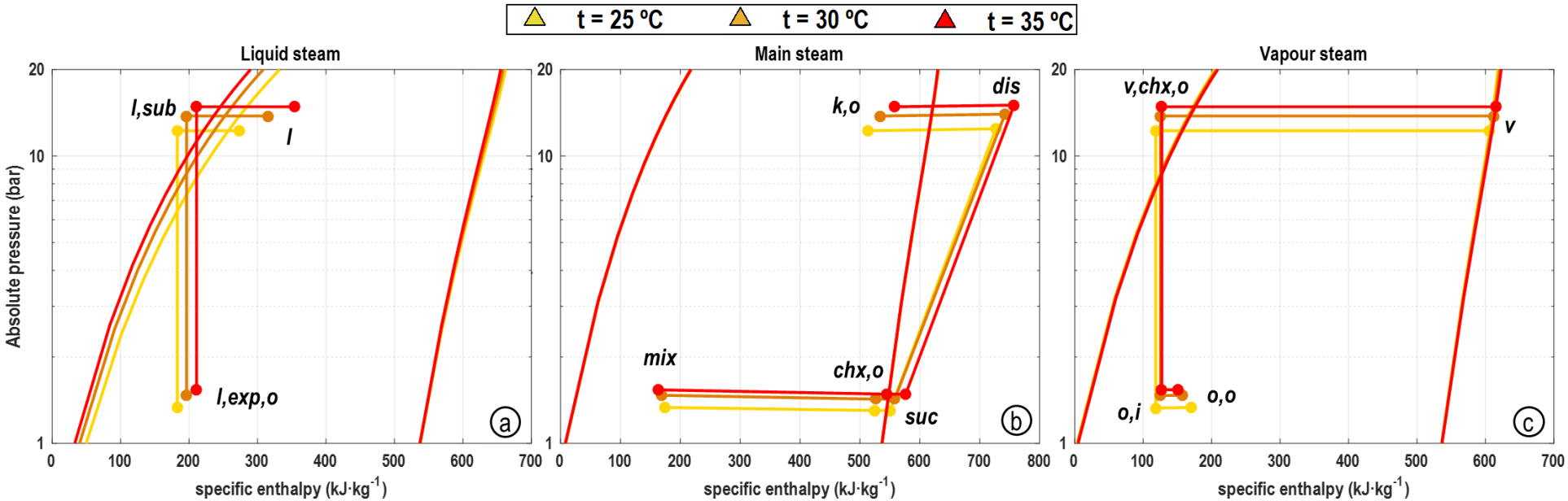

Fig. 9. Pressure-enthalpy diagrams of the three steams at t_{rs} = -79ºC at varius tenv. (a) corresponds to the liquid stream from the exit of the PHS, (b) corresponds to the circulating stream through the comperssor, (c) corresponds to the vapour steam at the exit of the PHS. (See operating conditions and compositions in Table 4 and Table 5)

4.2. Energy parameters

Finally, the analysis of steady-state operation of the AC system for the combination 340 g 30/70 % is extended to all the tested range, focusing only on the main energy parameters of the cycle. Uncertainty calculation of the main parameters is detailed in Annex 1.

Provided cooling capacity is evaluated as product of the vapour mass flow and the enthalpy difference in the evaporator, as detailed by Eq. (*4*). The AC is able to provide 179.5 ± 8.3 W (t_{rs} = -63.7ºC, t_{env} = 25ºC), to 86.0 ±15 W (t_{rs} = -79.0 ºC, t_{env} = 35 ºC). A high reduction of the capacity is observed as t_{env} increases. Although $\dot{m}_v$ increases with t_{env} and is slightly reduced with increased t_{rs}, the main cause of the capacity reduction is the shortage of the enthalpy difference in the evaporator. In this case, q_o goes from 122.5 kJ·kg^{-1} (t_{rs} = -63.7 ºC, t_{env} = 25 ºC) to 65.8 kJ·kg^{-1} (t_{rs} = -79.0 ºC, t_{env} = 35 ºC). COP reached by the AC system, evaluated as quotient between cooling capacity and compressor power consumption, Eq. (*5*), it has also a clear reduction dependence as increased t_{env} and decreased t_{rs}. The AC system reaches a maximum COP of 0.195 ± 0.009 (t_{rs} = -63.7 ºC, t_{env} = 25 ºC) and minimum of 0.087 ± 0.015 (t_{rs} = -79.0 ºC, t_{env} = 35 ºC). It needs to be mentioned that the COP uncertainty is large as lower t_{rs} and higher t_{env} are.

Measured COP values are low but are in the same order of magnitude those provided by other scientists with ultra-low-temperature systems. For example, Zhang et al. measured a COP of 0.52 for a Δt_{span} =88.3K at -70ºC [17] and Sobieraj of 0.16 for a Δt_{span} =85K at -60ºC [24]. However, all the experimental measurements are quite low in comparison with those coming from theoretical studies [Li et al. [13] COP=0.65 at Δt_{span} =110K at -80ºC / Rodriguez-Jara et al. COP=0.41 at Δt_{span} =101K at -80ºC]. One possible reason that explains the low COP values in relation to the theoretical could be the performance of the R404A compressor when used with the AC mixture. The circulating refrigerant flow through the compressor ($\dot{m}_t$) is around 26% than that of R404A at the same suction and discharge pressures. That results in low overall effectiveness of the compressor (calculated with Eq. (*6*) and detailed in Table 5), which vary for the operation at -80ºC between 35 to 42% approximately.

$$\dot{Q}_o = \dot{m}_v \cdot (h_{o,o} - h_{o,i}) \qquad \text{Eq. (4)}$$

$$COP = \frac{\dot{Q}_o}{P_C} \qquad \text{Eq. (5)}$$

$$\eta_g = \frac{m_t \cdot \left(h_{dis,S} - h_{suc}\right)}{P_C} \qquad \text{Eq. (6)}$$

The heat transfer in the CHX and IHX is evaluated through an iterative convergence procedure detailed by Llopis et al. [7] that assumes negligible heat losses with the environment. Thus, heat transfer in the CHX can be expressed through both steams as detailed by Eq. (7) and it is depicted in Fig. 12. Heat power ranges from 1236 ± 55 W (t_{rs} = -63.7 ºC, t_{env} = 25 ºC) to 1802 ± 164 W (t_{rs} = -79.0 ºC, t_{env} = 35 ºC), it being higher as higher t_{env} and lower t_{rs} are. This heat exchanger, acting as condenser and evaporator in the system, perform the highest heat transfer rate, it being between 6.6 (t_{rs} = -63.7ºC, t_{env} = 25ºC) to 20.8 (t_{rs} = -79.0ºC, t_{env} = 35ºC) times higher than the cooling capacity. Furthermore, the uncertainty associated with this parameter is high (from 4.5 to 9.1 %) since the evaporating steam is

always in two-phase condition. In relation to the heat transferred in the IHX, evaluated as well by a convergence procedure, expressed by Eq. (*8*) and depicted in Fig. 13, varies from 81 ± 5 W (t_{rs} = -83.4 ºC, t_{env} = 25 ºC) to 150 ± 7 W (t_{rs} = -59.2 ºC, t_{env} = 35 ºC). This parameter mainly depends on t_{env}.

$$\dot{Q}_{CHX} = \dot{m}_v \cdot (h_v - h_{v,chx,o}) = \dot{m}_l \cdot (h_{chx,o} - h_{mix}) \qquad \text{Eq. (7)}$$

$$\dot{Q}_{IHX} = \dot{m}_l \cdot (h_l - h_{l,sub}) = \dot{m}_t \cdot (h_{suc} - h_{chx,o}) \qquad \text{Eq. (8)}$$

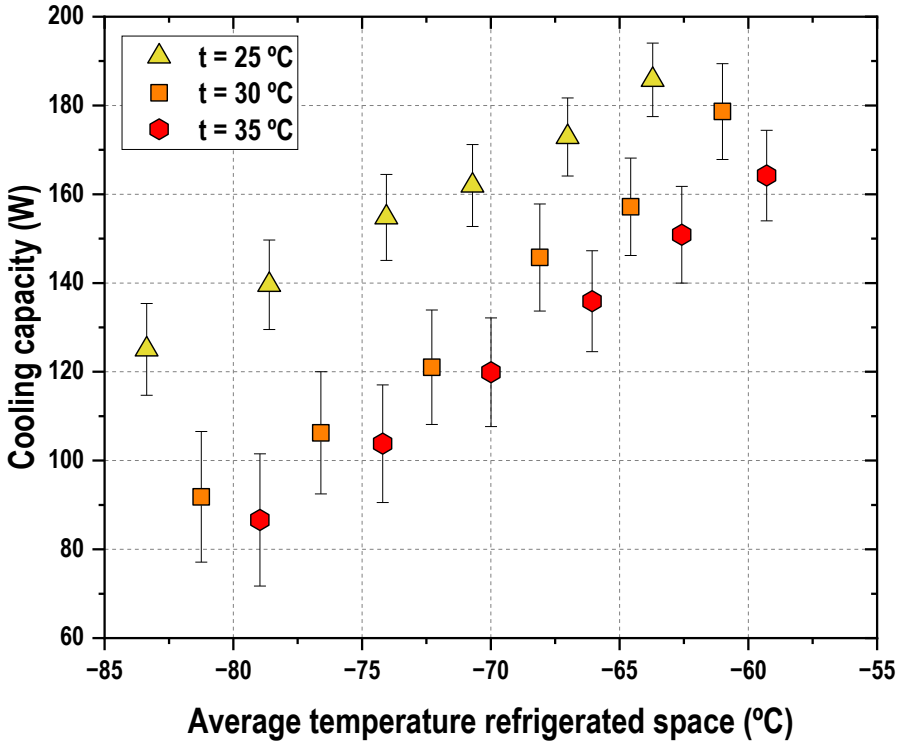

Fig. 10. Cooling capacity of 340 g R1150/R600a [30/70%]

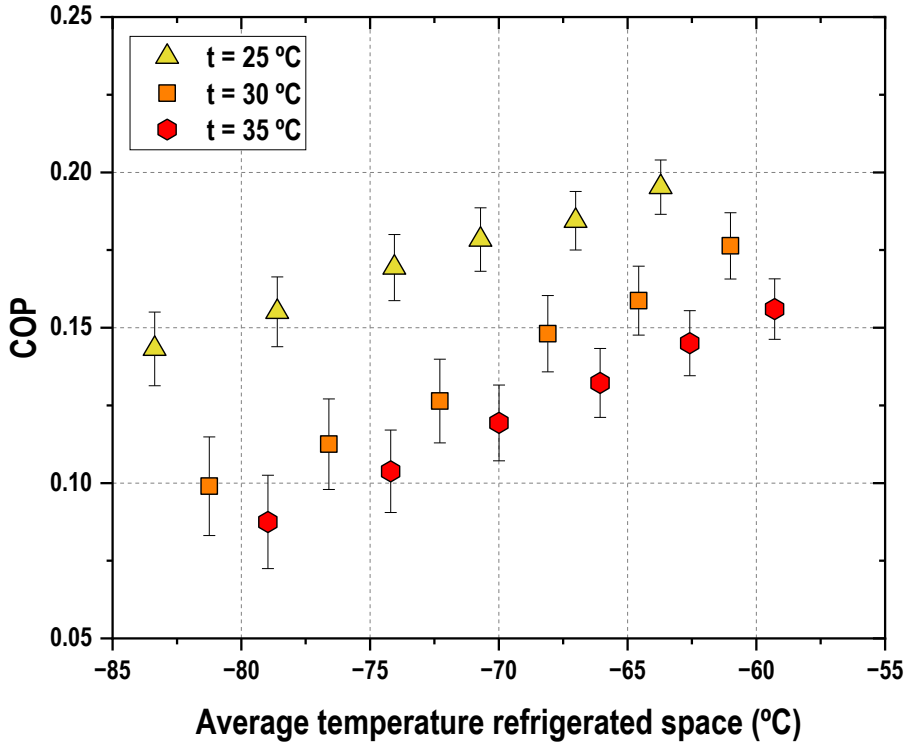

Fig. 11. COP of 340 g R1150/R600a [30/70%]

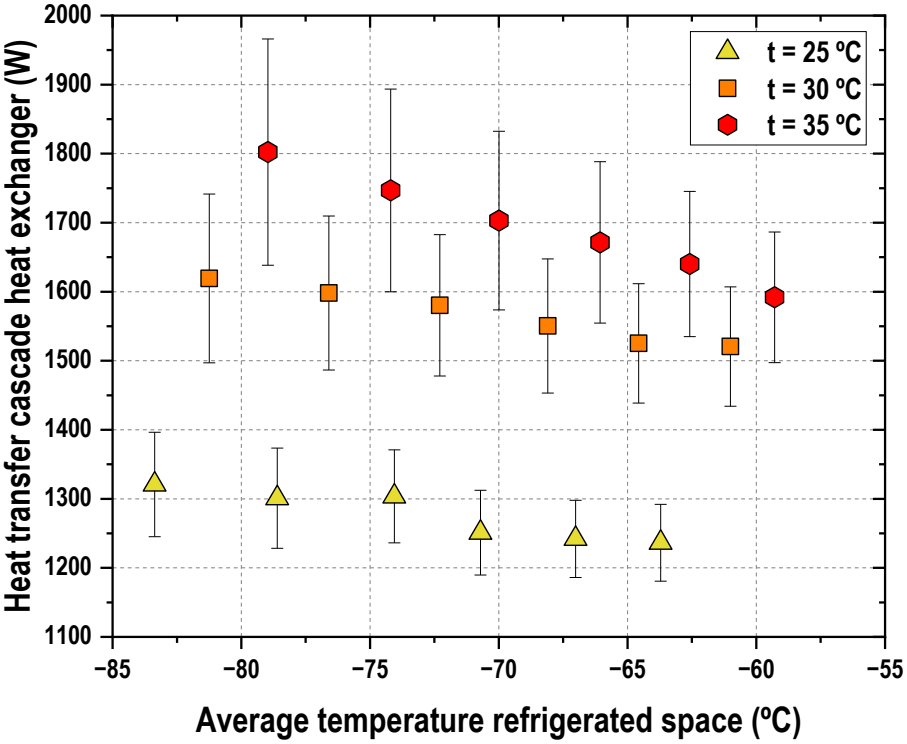

Fig. 12. Heat transfer cascade heat exchanger of 340 g R1150/R600a [30/70%]

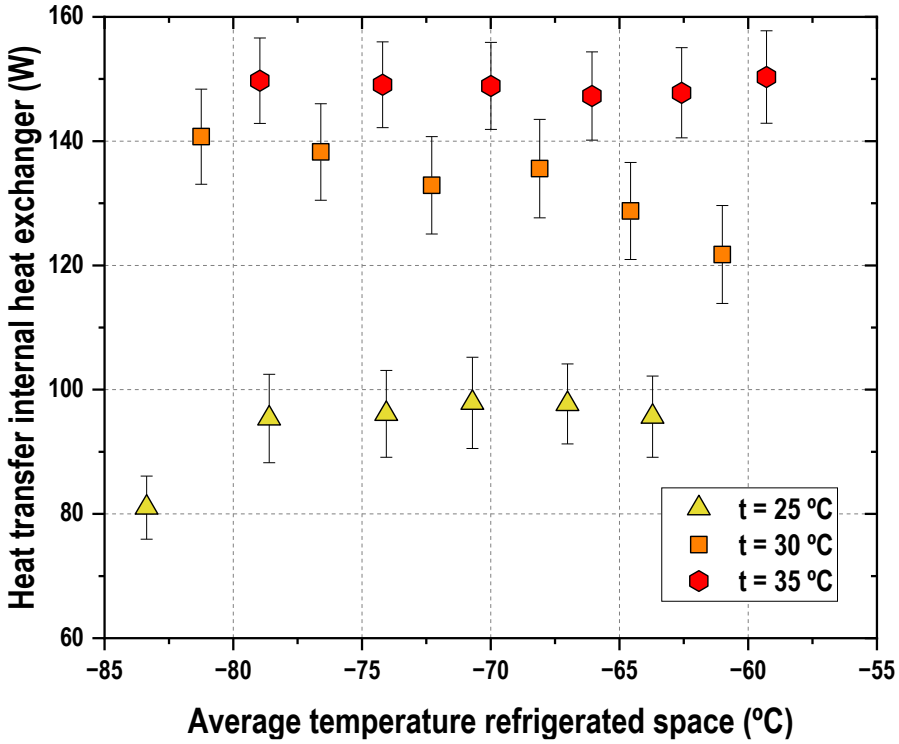

Fig. 13. Heat transfer in internal heat exchanger of 340 g R1150/R600a [30/70%]

5. Conclusions

This work presents the first comprehensive experimental evaluation of an auto-cascade refrigeration system designed to provide ultra-low temperatures (-80 ºC) using the hydrocarbons pair R1150/R600a. Considered system used a semihermetic compressor, a microchannel air condenser, a phase separator, a brazed plate heat exchanger, a double-tube heat exchanger, two capillaries and a refrigerated space, and it was fully instrumented to allow its thermodynamic characterization.

The plant was optimized in terms of energy consumption with three charging compositions (R1150/R600a) and different mass charges. Each configuration was subjected to 6-hour energy consumption tests inside a climatic chamber (t_{env}=25 ºC) covering temperatures of the refrigerated space from -80 to -60 ºC approximately. The plant was controlled using ON/OFF compressor regulation. From the combinations that allowed reaching a temperature in the refrigerated space below -80 ºC, the best performing combinations were 300 g and 340 g at 30/70 $\%_{mass}$ and 320 g at 35/65 $\%_{mass}$. Other combinations presented higher energy consumption, and in the case of the mixture at 25/75 $\%_{mass}$ a large duty cycle.

Combination 340 g 30/70 $\%_{mass}$ was subjected to a steady-state test covering temperatures of the refrigerated space from -83.4 to -59.3 ºC, at three heat rejection levels (25, 30 and 35 ºC) using a resistor placed inside the refrigerated space and controlled by a PWM control. Results were evaluated using a convergence iterative method developed by Llopis R. et al., that allowed to evaluate compositions, thermodynamic states, and energy parameters.

First important observation is that the circulating composition of the mixture greatly differs from the charging one. Circulating composition, which remained practically constant along all the tested range, presented larger proportion (43.2 to 44.9 $\%_{maxx}$) of R1150 than that of charging (30%). The hypothesis is that some R600a is retained in the heat exchangers (cascade heat exchanger and evaporator) at very low temperatures and does not circulate through the plant. In addition, both vapour and liquid steam compositions presented a dependence on the operating conditions. In relation to the vapour fractionated in the phase separator, the proportion of R1150 (the most volatile) decreases as higher the heat rejection level and lower the temperature in the refrigerated space are, thus, reducing the capacity to provide very low temperatures in the evaporator. In addition, the compositions in the phase separator agree with the equilibrium compositions calculated with Refprop v.10. They only differ when the liquid steam contain vapour, but they can be calculated through a mass balance.

Second, the energy parameters and their uncertainty were evaluated. Cooling capacity of the plant varied between 179.5 ± 8.3 W to 86.0 ±15 W. It was measured a large reduction of the capacity as the heat rejection level increased, mainly caused by the reduction of the specific cooling capacity in the evaporator. COP varied from 0.087 ± 0.015 to 0.195 ± 0.009; it has also a great dependence on the heat rejection level and the temperature of the refrigerated space. COP values are in the same order of magnitude to similar experimental works, but lower to those predicted from theoretical approximations. Use of a R404A for this application entails operation at low overall compressor efficiencies, from 35 to 41%, due to reduced mass flow rate, which could significantly affect to the energy performance of the AC system. Finally, the heat transfer rates in the internal heat exchangers of the plant were discussed. Although the heat power in the internal heat exchanger was in the same other of magnitude than the cooling capacity, the heat transfer rate in the cascade heat exchanger was between 6.6 to 20.8 times higher than the cooling capacity.

This work presents the first extensive experimental evaluation of a simple auto-cascade refrigeration system using the hydrocarbons R600a and R1150. The measured energy parameters were modest, but they were measured with a good degree of uncertainty. Therefore, the data provided in this work can be used to validate detailed models that will allow to modify the operating cycle and look for best energy performing architectures.

Acknowledgements

Grant TED2021-130162B-I00 funded by MCIN/AEI/ 10.13039/501100011033 and by "ERDF A way of making Europe" by the "European Union". Grant CIAEST/2021/14 funded by the Generalitat Valenciana. Authors want to acknowledge the economic support to this study by the European Union – "NextGenerationEU" (L. Nebot, Margarita Salas postdoctoral contract MGS/2022/15; M. E. Martínez, grant INVEST/2022/294 and by Jaume I University (D. Calleja, grant PREDOC/2019/19).

Author contributions

R. Ll. designed the test rig and its measurement system, developed the calculation method, and wrote the manuscript. M. M performed the experimental campaign and was responsible for the modifications and adaptations of the plant. L. N. and D.C. reviewed the manuscript.

References

[1] International Institute of Refrigeration, UNEP, Cold chain technology Brief: Vaccines, in, 2021.

[2] A. Mota-Babiloni, M. Mastani Joybari, J. Navarro-Esbrí, C. Mateu-Royo, Á. Barragán-Cervera, M. Amat-Albuixech, F. Molés, Ultralow-temperature refrigeration systems: Configurations and refrigerants to reduce the environmental impact, International Journal of Refrigeration, 111 (2020) 147-158.

[3] Y. Li, G. Liu, Q. Chen, G. Yan, Progress of auto-cascade refrigeration systems performance improvement: Composition separation, shift and regulation, Renewable and Sustainable Energy Reviews, 187 (2023) 113664.

[4] European Commission, Regulation (EU) No 517/2014 of the European Parliament and of the Council of 16 April 2014 on fluorinated greenhouse gases and repealing Regulation (EC) No 842/2006., (2014).

[5] J. Liu, Y. Liu, G. Yan, J. Yu, Theoretical study on a modified single-stage autocascade refrigeration cycle with auxiliary phase separator, International Journal of Refrigeration, 122 (2021) 181-191.

[6] E.Á. Rodríguez-Jara, F.J. Sánchez-de-la-Flor, J.A. Expósito-Carrillo, J.M. Salmerón-Lissén, Thermodynamic analysis of auto-cascade refrigeration cycles, with and without ejector, for ultra low temperature freezing using a mixture of refrigerants R600a and R1150, Applied Thermal Engineering, 200 (2022) 117598.

[7] R. Llopis, M. Martínez-Ángeles, M. García-Valero, A novel method to measure the energy efficiency and performance of an auto-cascade refrigeration cycle, Applied Thermal Engineering, (2023) 121146.

[8] Q. Wang, D.H. Li, J.P. Wang, T.F. Sun, X.H. Han, G.M. Chen, Numerical investigations on the performance of a single-stage auto-cascade refrigerator operating with two vapor–liquid separators and environmentally benign binary refrigerants, Applied Energy, 112 (2013) 949-955.

[9] Y. He, H. Wu, Y. Liu, T. Wang, X. Wu, C. Cheng, T. Jin, Theoretical performance comparison for two-stage auto-cascade refrigeration system using hydrocarbon refrigerants, International Journal of Refrigeration, (2022).

[10] G. Yan, J. Chen, J. Yu, Energy and exergy analysis of a new ejector enhanced auto-cascade refrigeration cycle, Energy Conversion and Management, 105 (2015) 509-517.

[11] G. Yan, H. Hu, J. Yu, Performance evaluation on an internal auto-cascade refrigeration cycle with mixture refrigerant R290/R600a, Applied Thermal Engineering, 75 (2015) 994-1000.

[12] J. Liu, Y. Liu, G. Yan, J. Yu, Thermodynamic analysis on a modified auto-cascade refrigeration cycle with a self-recuperator, International Journal of Refrigeration, (2022).

[13] D. Li, T. Bai, J. Yu, Thermodynamic performance optimization and analysis of an auto-cascade refrigeration cycle with vapor injection for ultra-low temperature freezer, International Journal of Refrigeration, 145 (2023) 425-435.

[14] Y. Tan, X. Li, L. Wang, L. Huang, Y. Xiao, Z. Wang, S. Li, Thermodynamic performance of the fractionated auto-cascade refrigeration cycle coupled with two-phase ejector using R1150/R600a at −80 °C temperature level, Energy, 281 (2023) 128328.

[15] C. Aprea, A. Maiorino, Autocascade refrigeration system: Experimental results in achieving ultra low temperature, International Journal of Energy Research, 33 (2009) 565-575.

[16] K. Du, S. Zhang, W. Xu, X. Niu, A study on the cycle characteristics of an auto-cascade refrigeration system, Experimental Thermal and Fluid Science, 33 (2009) 240-245.

[17] L. Zhang, S. Xu, P. Du, H. Liu, Experimental and theoretical investigation on the performance of CO2/propane auto-cascade refrigerator with a fractionation heat exchanger, Applied Thermal Engineering, 87 (2015) 669-677.

[18] T. Bai, G. Yan, J. Yu, Experimental investigation of an ejector-enhanced auto-cascade refrigeration system, Applied Thermal Engineering, 129 (2018) 792-801.

[19] T. Bai, G. Yan, J. Yu, Experimental research on the pull-down performance of an ejector enhanced auto-cascade refrigeration system for low-temperature freezer, Energy, 157 (2018) 647-657.

[20] E. Ángel Rodríguez-Jara, F. José Sánchez-de-la-Flor, J. Antonio Expósito-Carrillo, J. Manuel Salmerón-Lissén, Thermodynamic analysis of auto-cascade refrigeration cycles, with and without ejector, for ultra low temperature freezing using a mixture of refrigerants R600a and R1150, Applied Thermal Engineering, (2021) 117598.

[21] Lemmon E. W., B. I.H., H.M. L., M.M. O., NIST Standard Reference Database 23: Reference Fluid Thermodynamic and Transport Properties-REFPROP, Version 10.0, National Institute of Standards and Technology, (2018).

[22] B. Sreenivas, H.G. Nayak, G. Venkatarathnam, Relationship between composition of mixture charged and that in circulation in an auto refrigerant cascade and a J-T refrigerator operating in liquid refrigerant supply mode, Cryogenics, 81 (2017) 42-46.

[23] Q. Chen, G. Yan, J. Yu, Experimental research on the concentration distribution characteristics of dual-temperature refrigeration system using R290/R600a based on separation condensation, International Journal of Refrigeration, 131 (2021) 244-253.

[24] M. Sobieraj, M. Rosiński, High phase-separation efficiency auto-cascade system working with a blend of carbon dioxide for low-temperature isothermal refrigeration, Applied Thermal Engineering, 161 (2019).

Table 1. Measurement devices, range, and uncertainties

Measurement	Variables	Device	Range	Uncertainty
Liquid density	ρ_l	Coriolis mass flow meter	300 to 700 kg·m^{-3}	±0.2% of measurement
Pressure	p_{dis}, p_{phs}	Pressure gauge	0 to 31 bar$_{abs}$	±1% of measurement
Pressure	$p_{o,in}$, $p_{o,out}$, p_{suc}	Pressure gauge	0 to 9 bar$_{abs}$	±1% of measurement
Temperature	t_{suc}, t_{dis}, $t_{k,o}$, t_v, $t_{v,chx,o}$, t_l, $t_{l,sub}$, $t_{l,exp,o}$, t_{mix}, $t_{chx,o}$, t_{env}	Surface T-type thermocouple	-150 to 200 ºC	0.5 K
Temperature	$t_{o,i}$, $t_{o,o}$	4 surface T-type thermocouple	-150 to 200 ºC	0.25 K
Temperature refrigerated space	$t_{r,1}$, …, $t_{r,4}$	T-type thermocouple inside 25g brass cylinder	-150 to 200 ºC	0.5 K
Liquid mass flow rate	$\dot{m}_l$	Coriolis mass flow meter	0 to 12 kg·h^{-1}	±0.25% of measurement
Power consumption	P_c, P_{fan}	Digital wattmeter	0 to 4 kW	±0.5% of measurement

Table 2. Considered mixtures. Main properties of charging composition and main parameters fractionating at 15 and 20 bar at t_{env}=25ºC

Charging composition (by % mass)		Main fluid properties			Fractionation at 25ºC and 15 bar					Fractionation at 25ºC and 20 bar				
Z_{R600a}	Z_{R1150}	t_{crit}	p [a]	v_{suc} [b]	$x_{v_{k,o}}$ [c]	$Z_{R1150,vap}$ [d]	$t_{o,in}$ [e]	$q_{o,max}$ [f]	$q_{o,vol,max}$ [g]	$x_{v_{k,o}}$ [h]	$Z_{R1150,vap}$ [i]	$t_{o,in}$ [j]	$q_{o,max}$ [k]	$q_{o,vol,max}$ [l]
(%)	(%)	(ºC)	(bar)	($m^3 \cdot kg^{-1}$)	(-)	(%)	(ºC)	($kJ \cdot kg^{-1}$)	($kJ \cdot m^{-3}$)	(-)	(%)	(ºC)	($kJ \cdot kg^{-1}$)	($kJ \cdot m^{-3}$)
65	35	99.10	13.07	0.35	0.42	62.08	-88.55	119.80	41.81	0.26	70.67	-91.18	174.24	60.81
70	30	105.18	10.82	0.33	0.32	62.08	-88.55	119.80	40.09	0.16	70.67	-91.18	174.24	58.30
75	25	111.07	8.95	0.32	0.21	62.08	-88.55	119.80	38.36	0.05	70.67	-91.18	174.24	55.78

a) pressure at t_{env} = 25ºC and x_v=50% for composition through the condenser

b) suction volume at t=0ºC and p=1.5bar for composition through the compressor

c) vapour title or ratio $\dot{m}_v/\dot{m}_l$ at the exit of the condenser fractionating at 15 bar, [h) fractionating at 20 bar]

d) mass percentage of R1150 in the vapour steam fractionating at 15 bar, [i) fractionating at 20 bar]

e) inlet temperature to the evaporator for $t_{v,chx,o}$=-40ºC at 1.5 bar, [j) fractionating at 20 bar]

f) maximum specific cooling effect for $t_{v,chx,o}$=-40ºC and $t_{o,o}$=-80ºC at 1.5 bar, [k) fractionating at 20 bar]

g) maximum volumetric cooling effect for t_{suc}=0ºC at 1.5 bar, [l) fractionating at 20 bar]

Table 3. Operating parameters during cycling operation at different set point temperatures

		Set point = -80ºC				Set point = -70ºC				Set point = -60ºC			
		$p_{dis,max}$	$p_{suc,min}$	$t_{dis,max}$	$t_{o,mean}$*	$p_{dis,max}$	$p_{suc,min}$	$t_{dis,max}$	$t_{o,mean}$*	$p_{dis,max}$	$p_{suc,min}$	$t_{dis,max}$	$t_{o,mean}$*
Composition	*Charge (g)*	*(bar)*	*(bar)*	*(ºC)*	*(ºC)*	*(bar)*	*(bar)*	*(ºC)*	*(ºC)*	*(bar)*	*(bar)*	*(ºC)*	*(ºC)*
R1150/R600a [35/65%]	280	18.12	1.18	112.7	-86.3	20.93	1.27	103.9	-81.4	23.88	1.18	102.4	-72.8
	300	18.11	1.24	108.0	-84.9	21.14	1.34	102.5	-80.5	24.13	1.35	101.0	-74.0
	320	18.32	1.31	103.5	-85.1	21.41	1.39	100.7	-80.6	24.76	1.43	100.0	-74.6
R1150/R600a [30/70%]	300	16.37	1.10	101.3	-84.0	18.67	1.14	99.2	-79.6	22.21	1.03	97.4	-72.2
	340	19.36	1.17	96.3	-82.6	21.93	1.17	97.1	-79.0	24.69	1.16	96.0	-72.2
R1150/R600a [25/75%]	300	15.55	0.70	96.6	-84.9	16.68	0.79	94.3	-79.0	19.33	0.84	92.2	-71.5
	340	14.77	1.11	89.0	-81.9	17.91	1.03	92.1	-78.3	20.45	0.86	91.9	-71.7

*$t_{o,mean}$ corresponds to the mean temperature in the evaporator during compressor operation

Table 4. Steady-state temperature and pressure measurements for 340g at 30/70%$_{mass}$ at -79ºC of refrigerated space for different t_{env}

t_{env} (ºC)	t_{rs} (ºC)	t_{dis} (ºC)	$t_{k,out}$ (ºC)	$t_{v,chx,o}$ (ºC)	$t_{o,in}$ (ºC)	$t_{o,out}$ (ºC)	t_{suc} (ºC)	p_{suc} (bar)	p_{dis} (bar)
24.27	-78.60	92.69	24.29	-47.26	-91.18	-86.25	-23.69	1.30	12.43
30.12	-76.60	101.52	30.31	-43.88	-90.89	-84.12	-18.14	1.43	13.98
34.64	-78.97	109.52	34.84	-42.66	-89.40	-82.61	-5.98	1.48	15.03

Table 5. Steady-state compositions, vapour titles and energy parameters for 340g at 30/70%$_{mass}$ at -79ºC of refrigerated space for different t_{env}

t_{env} (ºC)	$Z_{t_{R1150}}$ (%)	$Z_{v_{R1150}}$ (%)	$Z_{l_{R1150}}$ (%)	$\dot{m}_t$ (kg/h)	$\dot{m}_l$ (kg/h)	$\dot{m}_v$ (kg/h)	η_g (%)	$x_{v_{k,out}}$ (-)	x_{v_l} (-)	$x_{v_{o,in}}$ (-)	$x_{v_{o,out}}$ (-)	$\dot{Q}_o$ (W)	$\dot{Q}_{CHX}$ (W)	$\dot{Q}_{IHX}$ (W)	$\dot{Q}_k$ (W)	P_C (W)	COP (-)
24.27	43.7	55.9	12.7	8.57	3.68	4.89	35.0	0.72	0.03	0.206	0.305	139.6	1301.0	95.4	795.9	900.0	0.155
30.12	43.8	53.6	16.2	8.90	3.87	5.03	35.8	0.77	0.10	0.209	0.270	106.3	1598.1	138.3	926.9	944.3	0.113
34.64	44.4	51.5	19.4	10.15	4.00	6.15	41.6	0.82	0.19	0.205	0.250	86.6	1802.3	149.7	944.6	990.1	0.087

Annex 1. Uncertainty calculation

Energy performance and heat transfer rates in the cycle are evaluated using an iterative procedure, as detailed by Llopis et al. [7]. The uncertainty calculation of each parameter is made by computing the deviation in the results considering the measurement errors of used sensors.

The liquid composition at the exit of the PHS, which depends only on three measurements ($p_{phs}, t_{l,sub}, \rho_l$), Eq. (A. 1), is evaluated with Refprop v.10 [21], and its uncertainty considering the deviation of the three variables, as detailed by Eq. (A. 2). Particular deviation is calculated as the arithmetical mean of the deviation caused by the error of each sensor, as detailed by Eq. (A. 3) to (A. 5).

$$Z_l = f(p_{phs}, t_{l,sub}, \rho_l) \tag{A. 1}$$

$$I_{Z_l} = \sqrt{{I_p}^2 + {I_t}^2 + {I_\rho}^2} \tag{A. 2}$$

$$I_p = \frac{\left|Z_{l_{p+}} - Z_{l_o}\right| + \left|Z_{l_{p-}} - Z_{l_o}\right|}{2} = \frac{\left|f(p + \varepsilon_p, t, \rho_l) - Z_{l_o}\right| + \left|h(p - \varepsilon_p, t, \rho_l) - Z_{l_o}\right|}{2} \tag{A. 3}$$

$$I_t = \frac{\left|Z_{l_{t+}} - Z_{l_o}\right| + \left|Z_{l_{t-}} - Z_{l_o}\right|}{2} = \frac{\left|f(p, t + \varepsilon_t, \rho_l) - Z_{l_o}\right| + \left|f(p, t - \varepsilon_t, \rho_l) - Z_{l_o}\right|}{2} \tag{A. 4}$$

$$I_\rho = \frac{\left|Z_{l_{\rho+}} - Z_{l_o}\right| + \left|Z_{l_{\rho-}} - Z_{l_o}\right|}{2} = \frac{\left|f(p, t, \rho_l + \varepsilon_\rho) - Z_{l_o}\right| + \left|f(p, t, \rho_l - \varepsilon_\rho) - Z_{l_o}\right|}{2} \tag{A. 5}$$

This procedure is extended to all the energy parameters considered in this work considering the deviation of the 11 measurements used in the calculation model and the uncertainty for each parameter is calculated using Eq. (A. 6) where the deviation caused by each sensor is computed with Eq. (A. 7). In this equation, X_o is the calculation with the measurement value; X_{j+} the calculated value with the measurement value plus the uncertainty of the device; and X_{j-} the calculated value with the measurement value minus the uncertainty of the device.

$$I_i = \sqrt{\sum_{j=1}^{11} {I_j}^2} \tag{A. 6}$$

$$I_j = \frac{\left|X_{j+} - X_o\right| + \left|X_{j-} - X_o\right|}{2} \tag{A. 7}$$